Received: 10 September 2020 | Revised: 21 December 2020 | Accepted: 28 December 2020

DOI: 10.1002/cm.21650

SHORT REPORT

Switch-1 instability at the active site decouples ATP hydrolysis from force generation in myosin II

Benjamin C. Walker[1] | Claire E. Walczak[2] | Jared C. Cochran[1]

[1]Department of Molecular & Cellular Biochemistry, Indiana University, Bloomington, Indiana

[2]Medical Sciences, Indiana University School of Medicine-Bloomington, Bloomington, Indiana

Correspondence
Claire E. Walczak, Indiana University School of Medicine-Bloomington, Medical Sciences, Bloomington, IN 47405.
Email: cwalczak@indiana.edu

Present address
Jared C. Cochran, 1300 N. Patterson Dr., Bloomington, Indiana

Funding information
National Science Foundation, Grant/Award Number: MCB 1614514; School of Optometry at Indiana University; Indiana School of Medicine-Bloomington; Office of the Vice Provost for Research, College of Arts and Sciences; The work was funded by the NSF grant. All of the other funding sources supported the imaging center but not directly to the project

Abstract

Myosin active site elements (i.e., switch-1) bind both ATP and a divalent metal to coordinate ATP hydrolysis. ATP hydrolysis at the active site is linked via allosteric communication to the actin polymer binding site and lever arm movement, thus coupling the free energy of ATP hydrolysis to force generation. How active site motifs are functionally linked to actin binding and the power stroke is still poorly understood. We hypothesize that destabilizing switch-1 movement at the active site will negatively affect the tight coupling of the ATPase catalytic cycle to force production. Using a metal-switch system, we tested the effect of interfering with switch-1 coordination of the divalent metal cofactor on force generation. We found that while ATPase activity increased, motility was inhibited. Our results demonstrate that a single atom change that affects the switch-1 interaction with the divalent metal directly affects actin binding and productive force generation. Even slight modification of the switch-1 divalent metal coordination can decouple ATP hydrolysis from motility. Switch-1 movement is therefore critical for both structural communication with the actin binding site, as well as coupling the energy of ATP hydrolysis to force generation.

KEYWORDS
hydrolase, kinetics, molecular motor, RRID:SCR_002285, RRID:SCR_006643

1 | INTRODUCTION

Myosins and kinesins are structurally related cytoskeletal molecular motors that use the free energy of ATP hydrolysis to produce force along filament tracks (filamentous actin or microtubules) and play essential roles for a diverse range of cellular processes. The conversion of chemical energy at their active sites to mechanical energy at the filament binding interface and force producing elements is facilitated by conformational changes in their structurally similar central core (Cochran, 2015; Kull & Endow, 2002; Kull, Sablin, Lau, Fletterick, & Vale, 1996; Kull, Vale, & Fletterick, 1998; Robert-Paganin, Pylypenko, Kikuti, Sweeney, & Houdusse, 2020; Sack, Kull, & Mandelkow, 1999; Vale & Milligan, 2000).

Myosins and kinesins have three primary active site elements in their central core that are necessary for nucleotide and divalent metal binding (usually Mg^{2+}) to coordinate efficient ATP hydrolysis (Figure 1a) (Vale, 1996). The P-loop (Walker A motif) binds nucleotide and coordinates Mg^{2+}, and the switch-1 and switch-2 (Walker B motif) motifs sense and respond to the absence/presence of the γ-phosphate of the bound nucleotide via direct interaction with the nucleotide and Mg^{2+} (Vale & Milligan, 2000). Mg^{2+} at the active site is coordinated by the hydroxyl group of the serine/threonine residue in the P-loop, the oxygen from the β-phosphate of the bound nucleotide, and two water molecules (Figure 1a). The remaining two ligand elements necessary to satisfy the octahedral coordination geometry of Mg^{2+} depend on the

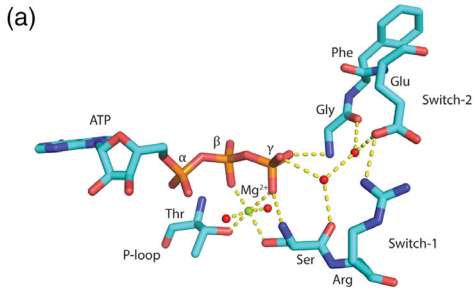

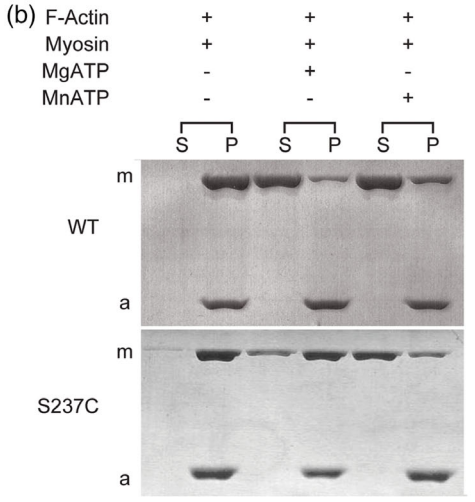

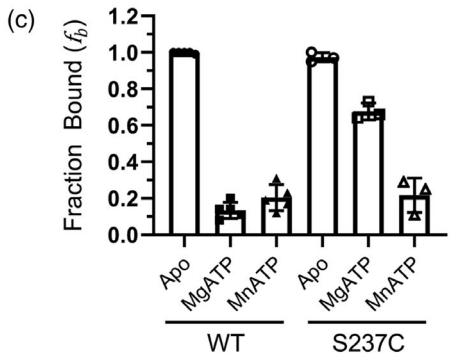

	WT (f_b)	S237C (f_b)
Apo	1.00 ± 0.00	0.97 ± 0.03
MgATP	0.13 ± 0.04	0.68 ± 0.05
MnATP	0.20 ± 0.07	0.22 ± 0.09

FIGURE 1 WT and S237C myosin cosedimentation with F-actin. (a) Divalent metal coordination of the ATP hydrolysis competent state in myosin. AMPPNP from a hydrolysis competent myosin II structure (PDB: 3MYK) was replaced with ATP from another myosin structure (PDB: 1FMW), after alignment using the P-loop residues. The magnesium ion is shown as a green sphere and water molecules are shown as red spheres. The yellow dotted lines represent polar contacts. (b) Representative Coomassie Blue-stained SDS-PAGE gel of WT or S237C myosin (1 μM) binding to phalloidin-stabilized F-actin (1.5 μM). Equivalent volumes of the supernatant (S) and pellet (P) fractions were electrophoresed from each reaction and quantified by densitometry (see panel C and table). Myosin is indicated with *m* and actin with *a*. (c) Bar graph and table representing the mean fraction ± *SD* of WT (n = 5) and S237C (n = 3) myosin bound (f_b) to F-actin [Color figure can be viewed at wileyonlinelibrary.com]

specific nucleotide state (nucleoside diphosphate or nucleoside triphosphate). Therefore, the metal ion anchors a network of important interactions in the enzyme that are necessary for efficient nucleotide hydrolysis.

For myosins and kinesins to produce work, movement of switch-1 and switch-2 loops at the active site are linked to the filament binding interface and force generating elements via structural changes in the central core (Vale & Milligan, 2000). These conformational changes modulate motor-filament affinity and movement of force producing elements, such as the lever arm in myosin and the neck linker in kinesin that allow for motor motility. Although kinesin and myosins share significant structural similarities, their thermodynamic and kinetic mechanisms differ. In myosins, ATP binding leads to rapid actomyosin dissociation followed by ATP hydrolysis (Kurzawa & Geeves, 1996); while in kinesins, ATP binding does not dissociate the tight kinesin-microtubule complex, and hydrolysis occurs before detachment (Gilbert, Webb, Brune, & Johnson, 1995). However, in both enzymes the rate limiting steps are stimulated by filament binding (Cochran, 2015).

Force generation by actomyosin occurs via cyclic interactions of filamentous actin (F-actin) and myosin that are mechanochemically coupled to its ATP hydrolysis cycle (Lymn & Taylor, 1971). How active site motifs are mechanochemically coupled to actin binding and the power stroke remain an area of active research. ATP binding to the active site results in closure of the nucleotide pocket through movements of the switch-1, switch-2, and P-loop motifs (Bobkov, Sutoh, & Reisler, 1997; Hiratsuka, 1994). Closure of the switch-1 loop onto the γ-phosphate of ATP is directly coupled to opening of the actin binding cleft and weakening of filament affinity (Conibear, Bagshaw, Fajer, Kovacs, & Malnasi-Csizmadia, 2003; Holmes, Angert, Kull, Jahn, & Schroder, 2003; Naber, Malnasi-Csizmadia, Purcell, Cooke, & Pate, 2010). Switch-2 closure, on the other hand, is coupled to the recovery stroke of the lever arm when dissociated from F-actin (Fischer, Windshugel, Horak, Holmes, & Smith, 2005; Koppole, Smith, & Fischer, 2007). Closure of the switches around ATP leads to rapid hydrolysis and subsequent rebinding of F-actin. How switch loop opening and product release of actomyosin are coupled to force generation is controversial and poorly understood (Gyimesi et al., 2008; Llinas et al., 2015; Muretta, Rohde, Johnsrud, Cornea, & Thomas, 2015; Woody, Winkelmann, Capitanio, Ostap, & Goldman, 2019).

In a previous study, we were able to control the enzymatic activity and F-actin binding of the core motor domain of *Dictyostelium discoideum* myosin II (M761) by substituting the divalent metal coordinating switch-1 serine (S237) with cysteine, which has diminished affinity for the Mg^{+2} metal, and thus inhibits its ATPase activity (Cochran, Thompson, & Kull, 2013). Substituting Mg^{+2} with Mn^{+2}, which strongly interacts with cysteine, restores metal interaction, ATPase activity, and actin binding. Hence exchanging divalent metals provided a direct and experimentally reversible link between switch-1 and the actin binding cleft. In addition to affinity, the atomic radii of the divalent metal seem to affect myosin ATPase activity and therefore switch-1 stability (Nihei & Tonomura, 1959). Ca^{2+} has a significantly higher radius than Mg^{2+} and Mn^{2+} and is the most well studied

metal ion besides Mg^{2+} and Mn^{2+} in relation to myosin activity and function. Ca^{2+} is therefore an obvious choice to further probe the effect switch-1/metal coordination on myosin ATPase activity and motility. Interestingly, the basal ATPase rate of wild type (WT) myosin in the presence of divalent metals other than Mg^{2+} is very high, which is similar to the high basal rates observed with the S237C mutant (Cochran et al., 2013). In addition, substituting Ca^{2+} leads to high basal ATPase rates that were inhibited in the presence of F-actin for both WT and S237C. This suggests that perturbing the switch-1 and divalent metal coordination leads to substantial structural instability at the active site with switch loops rapidly opening and closing for ATP hydrolysis and product release. How interference with switch-1 at the active site affects force generation is unknown.

Given that switch loop movement and product release are tightly coupled to the power stroke and force generation, we hypothesized that destabilizing switch-1 movement would negatively affect the tight coupling of ATP hydrolysis to force production that results in motility. To test this hypothesis, we fused two α-actinin repeats (2R) that function as an artificial lever arm necessary for motility (Anson, Geeves, Kurzawa, & Manstein, 1996) to the core motor domains of M761 and M761(S237C) used in our previous study (Cochran et al., 2013). Cosedimentation and steady-state ATPase assays confirmed that the α-actinin repeats did not change the behavior of the steady-state motor properties of the wild-type (WT) constructs. F-actin gliding assays indicated that WT myosin motility was reduced in the presence of Mn^{2+} compared to Mg^{2+} and absent in the presence of Ca^{2+}. On the other hand, the mutant failed to produce motility under all divalent metal conditions despite robust ATPase activity in the gliding chambers.

Together our results support a model whereby switch-1 coordination of the divalent metal at the active site directly regulates actin binding and force generation. Even slight modification of the switch-1 and divalent metal interaction has significant effects on ATP hydrolysis and can decouple hydrolysis from force generation. Switch-1 movement is therefore critical for allosteric communication with the F-actin binding cleft, as well as for coupling ATP hydrolysis to force generation.

2 | METHODS

Cloning, expression, and purification of M761(WT)-2R and M761 (S237C)-2R. The pDXA-3H plasmid encoding the wild-type (WT) soluble head fragment (amino acids 2–761) of *Dictyostelium discoideum* myosin II with two α-actinin repeats, M761(WT)-2R (116.3 kDa), was a generous gift from the Manstein lab (Kliche, Fujita-Becker, Kollmar, Manstein, & Kull, 2001). To generate the myosin II soluble head fragment with the S237C mutation, M761(S237C) (Cochran et al., 2013) was digested with *Bam*HI and *Bst*XI, and the resulting fragment was ligated into the M761(WT)-2R background to generate M761(S237C)-2R. All clones were confirmed by sequencing. For protein expression, M761(WT)-2R and M761(S237C)-2R were transfected into *D. discoideum* AX3-ORF+ cells (dictyBase, Cat# DBS0235546, RRID: SCR_006643) using electroporation as described (Gaudet, Pilcher, Fey, & Chisholm, 2007). Subconfluent plates of transformed *D. discoideum* were used to seed 0.5 L of AX medium (Formedium, Cat# AXM0102) in 2 L flasks at 10^5 cells/ml. Cultures were grown at 21°C and 120 rpm to 10^7 cells/ml before harvesting by centrifugation.

The M761(WT)-2R was purified as described with modifications (Cochran et al., 2013). Specifically, cells from ~1 L culture were resuspended in 60 ml of lysis buffer (50 mM Tris–HCl pH 8.0, 2 mM EDTA, 0.2 mM EGTA, 1 mM DTT, 5 mM benzamidine, 0.1 mM phenylmethylsulphonyl fluoride (PMSF), 1 tablet of cOmplete™ Protease Inhibitor Cocktail (Roche Applied Science, Cat# 11697498001), 2% (v/v) Triton X-100, 30 μg/ml RNase A, 1.7 U/ml units of alkaline phosphatase) and lysed for 15 min at 4°C. The cell lysate was clarified by centrifugation at 186,000 *g* and 4°C for 45 min. The cytoskeletal pellet was homogenized with 100 ml of extraction buffer (50 mM Na-HEPES pH 7.3, 100 mM NaCl, 30 mM potassium acetate, 10 mM magnesium acetate, 5 mM benzamidine, 0.1 mM PMSF, 1 tablet of cOmplete™ Protease Inhibitor Cocktail). Clarification and homogenization were repeated with 20 ml extraction buffer containing 20 mM ATP to release the myosin motor from actin. A final 370,000 x *g* centrifugation at 4°C for 45 min yielded a myosin-containing supernatant that was loaded onto a 1 ml nickel-nitrilotriacetic acid agarose (Ni-NTA) (Qiagen, Cat# 30210) column equilibrated with column buffer (50 mM Tris–HCl pH 8.0, 150 mM NaCl, and 1 mM EDTA, 30 mM imidazole). The protein was eluted from the column with elution buffer (column buffer, 0.47 M imidazole) and adjusted to 5 mM EDTA to chelate trace divalent cations. The eluted protein was incubated at 4°C for 15 min before buffer exchange with a HiPrep 26/10 resin column into final buffer (20 mM Na-HEPES pH 7.3, 95 mM potassium acetate, 0.1 mM EDTA, 150 mM sucrose, and 1 mM DTT) and concentrated using a 10 kDa Amicon® centrifuge filter (Millipore, Cat# C7715). Purified protein was flash frozen in liquid nitrogen and stored at −80°C. For the M761(S237C) protein, 10 mM $MnCl_2$ was added to the extraction buffer. Protein concentrations were determined using the Bradford Reagent (Sigma, Cat# B6916), SDS-PAGE densitometry, and absorption at A_{280} using 96,150 M^{-1} cm^{-1} as the extinction coefficient.

Preparation of F-actin. Chicken skeletal muscle G-actin was prepared from acetone powder as described (Spudich & Watt, 1971). G-actin was polymerized (F-actin) as described previously and stabilized by addition of phalloidin or fluorescein isothiocyanate (FITC) labeled phalloidin (Sigma Aldrich) in DMSO to a final molar concentration equal to or greater than F-actin (Cochran et al., 2013). Stabilized F-actin was pelleted at 214,000 x *g* for 40 min and resuspended in ATPase Buffer (20 mM Na-HEPES pH 7.2, 0.25 M KCl, 150 mM sucrose, 1 mM DTT).

Actomyosin Cosedimentation Assays. Actomyosin cosedimentation experiments were performed by mixing myosin with phalloidin stabilized F-actin at the indicated concentrations in reaction buffer (20 mM Na-HEPES pH 7.2, 5 mM $MgCl_2$, 250 mM KCl, 150 mM sucrose, 1 mM DTT) followed by incubation at 25°C for 10 min before the addition of either 10 mM MgATP or MnATP. After addition of

nucleotide, solutions were immediately pelleted by centrifugation at 100,000 x *g* for 15 min at 25°C. Supernatants were removed, and pellets were resuspended in an equal volume of reaction buffer. Gel samples were prepared from equivalent volumes of supernatant and pellet fractions for each reaction by the addition of 5X Laemli buffer (60 mM Tris–HCl pH 6.8, 0.4% w/v SDS, 10% v/v glycerol, 5% v/v β-mercaptoethanol, 0.01% w/v bromophenol blue) and analyzed by SDS-PAGE. Gels were stained with Coomassie, and densitometry was performed using the software FIJI (https://fiji.sc, RRID:SCR_002285) (Schindelin et al., 2012).

Steady-state NADH-coupled ATPase assays. Steady-state ATPase activities were monitored using the NADH coupled assay in modified reaction buffer (20 mM Na-HEPES pH 7.2, 100 mM KCl, 150 mM sucrose, 1 mM DTT) at 25°C (De La Cruz, Sweeney, & Ostap, 2000; Hass, Boyer, & Reynard, 1961; Imamura, Tada, & Tonomura, 1966). Briefly, 0.2 μM myosin in modified reaction buffer was mixed with an equal volume of NADH cocktail (1 mM ATP, 5 mM $MgCl_2$ or $MnCl_2$ or $CaCl_2$, 0.4 mM NADH (Acros Organic, Cat# 271100010), 0.5 mM phosphoenolpyruvate (Tokyo Chemical Industry), 5 U/ml rabbit pyruvate kinase (Roche Diagnostics, Cat# 10128155001), 8 U/ml lactate dehydrogenase (Sigma-Aldrich)), and an equal volume of F-actin or modified reaction buffer. After mixing, reactions were transferred into a 384-well plate in duplicate, pulse centrifuged at 1000 x *g*, and placed in a microplate spectrophotometer (BioTek) where NADH oxidation was monitored at 340 nm over time. The amount of NADH oxidized (which equals the amount of ADP produced) was calculated using a NADH standard curve (0 μM – 800 μM NADH). The NADH stocks and standard curves were confirmed by using the extinction coefficient of NADH (6,220 M^{-1} cm^{-1}) at 340 nm.

F-actin gliding assays. Gliding assays were performed as described with modifications (Kron, Toyoshima, Uyeda, & Spudich, 1991). All experiments were performed in motility buffer which contained either 20 mM MOPS pH 7.5 or 25 mM Na-HEPES pH 7.5, 25 mM KCl, 1 mM EGTA, 1 mM DTT. HEPES was used instead of MOPS after determining no effect on motility (data not shown). Incubations were performed in a humid container at 4°C. Briefly, myosin (50–-100 μg/ml) was infused in a nitrocellulose treated glass chamber and incubated for 5 min. Flow chambers held ~10 μl of solution. An additional two chamber volumes of myosin were wicked through the chamber and incubated for ≥5 min. The flow chamber was washed with two chamber volumes of blocking buffer (motility buffer, 0.5 mg/ml BSA) and incubated for 1 min. Two chamber volumes of F-actin (motility buffer, 0.5 mg/ml BSA, 0.01 μM FITC-labeled F-actin) were then wicked through the chamber and incubated for 2 min. Excess F-actin was washed out of the chamber by infusing two chamber volumes of wash buffer (motility buffer, 0.5 mg/ml BSA, oxygen scavenger system (25 mM glucose, 0.2 mg/ml glucose oxidase, 175 μg/m catalase, 71.6 mM β-mercaptoethanol) at 25°C. Static F-actin filaments were imaged using a Nikon NiE epifluorescence microscope equipped with a Plan Apo VC 60X 1.4 NA oil objective and a Hamamatsu Orca-Flash 2.8 sCMOS camera controlled by Nikon Elements software. To activate gliding, chambers were infused with two chamber volumes of gliding buffer (motility buffer, oxygen scavenger system, 20 U/ml pyruvate kinase, 2.5 mM phosphoenolpyruvate, 0.3% w/v methylcellulose (4,000 cP), 2 mM ATP, 2 mM of divalent metal ($MgCl_2$, $MnCl_2$, or $CaCl_2$)) and sealed with VALAP. Time-lapse images were recorded in 2–10 sec intervals. Images and movies were acquired with identical exposures and scaled identically in FIJI.

Gliding chamber ATPase assays. To measure the amount of ATP hydrolysis in gliding chambers, we recreated the gliding assay as described above with minor modifications. Gliding chambers accommodate ~20 μl volume. A modified gliding buffer was used (motility buffer, oxygen scavenger system, 20 U/ml rabbit pyruvate kinase, 2.5 mM phosphoenolpyruvate, 0.4 mM NADH, 8 U/ml lactate dehydrogenase, 2 mM ATP, 2 mM of divalent metal [$MgCl_2$ or $MnCl_2$]). The reaction was incubated at 25°C for 45 min. Subsequently, 30 μl of solution was extracted from the chamber by simultaneously pipetting the modified gliding buffer into one end of the chamber while extracting solution from the other end via suction. The extracted solution was immediately transferred into a 384-well plate and absorption at 340 nm was recorded using a microplate spectrophotometer. Every microscope slide contained two chambers, one where myosin was infused and the other where BSA was infused. Values obtained from the BSA control chambers were subtracted from values obtained from the myosin containing chambers.

3 | RESULTS & DISCUSSION

3.1 | The M761-2R S237C mutant can rescue F-actin release in the presence of MnATP

To study the effects of divalent metal coordination of nucleotide binding on myosin force production, we mutated serine 237 to cysteine (S237C) in myosin M761 (S1dC fragment of *Dictyostelium discoideum* myosin II) containing two α-actinin repeats (M761-2R) that act as lever arms to allow for motility. The WT and S237C constructs were expressed with a C-terminal 8x HIS purification tag in *D. discoideum*. Purification of the WT and S237C constructs yielded approximately 0.3 mg and 0.1 mg per liter of media, respectively, with >95% purity as determined by SDS-PAGE densitometry (Figure S1).

Actomyosin cosedimentation assays were performed to determine the fraction of M761-2R WT or S237C bound to phalloidin-stabilized F-actin under different metal conditions (Figure 1). Myosin and F-actin were brought to equilibrium before addition of metal-ATP and immediate centrifugation to capture the myosin fraction dissociated by ATP binding. In the absence of added nucleotide (apo), ≥95% of WT and S237C was bound to F-actin, consistent with a very low $K_{d,actin}$ previously reported (Kurzawa, Manstein, & Geeves, 1997) (Figure 1b,c). Upon addition of MgATP or MnATP, a large fraction of the WT protein detached from F-actin (f_b = 0.13 ± 0.04 and f_b = 0.20 ± 0.07, respectively), representing a weakening of actin binding by ~100 fold (Figure 1c). In contrast, the S237C mutant retained relatively tight binding in the presence of MgATP (f_b = 0.68 ± 0.05), and detachment was rescued in the presence of MnATP (f_b = 0.22 ± 0.09). As expected, these results are consistent with

previously published studies with M761 WT and S237C constructs without the α-actinin repeats, and directly reflect the change in affinity for the nucleotide where the S237C binds MgATP more than four orders of magnitude more weakly ($K_{m,ATP}$ = 7,800 μM) compared to WT ($K_{m,ATP}$ = 0.38 μM) but binds MnATP ($K_{m,ATP}$ = 70 μM) at the same order of magnitude as the WT ($K_{m,ATP}$ = 11.5 μM) (Cochran et al., 2013). Our results confirm that the S237C substitution in M761-2R appears to modulate the actomyosin interaction base on the divalent metal present in solution. This suggests that serine (–OH) in the WT switch-1 binds Mg^{2+} and Mn^{2+} sufficiently tightly to affect the release from F-actin, while the cysteine (–SH) in S237C can only bind Mn^{2+} well enough for efficient F-actin release.

3.2 | F-actin inhibition of the M761-2R S237C mutant with MgATP and CaATP is rescued by MnATP

To examine how changes in metal coordination affected catalytic activity, we performed NADH-coupled ATPase assays and determined the steady-state ATP turnover kinetics of WT and S237C M761-2R under different metal conditions (Figure 2). Our results with M761-2R constructs were consistent with previously published M761 data (Cochran et al., 2013). The ATPase rate of WT protein was slow in the presence of MgATP (0.02 ± 0.01 s^{-1}) and showed weak activation in the presence of 10 μM F-actin (0.08 ± 0.01 s^{-1}) (Figure 2a,b). In comparison WT ATP turnover was fast in the presence of Mn^{2+} (1.00 ± 0.13 s^{-1}) and Ca^{2+} (0.31 ± 0.14 s^{-1}), with no statistically significant F-actin stimulation, consistent with a weak F-actin affinity.

Previous studies found that divalent metals have an inhibitory effect on myosin basal ATPase (Malik, Marchioli, & Martonosi, 1972), yet Mg^{2+} stimulates the actomyosin complex ATPase activity (Burke, Reisler, & Harrington, 1973; Kobayashi, Ramirez, & Warren, 2019). The inhibitory effect of divalent metals on basal ATPase rate is likely due to inhibition of product release, given that the metal is coordinated by both the hydrolysis products and the switch-loops (Swenson et al., 2014). Therefore, the fast basal ATPase rates with Mn^{2+} and Ca^{2+} that we report here and elsewhere (Cochran et al., 2013) are probably caused by a much more dynamic switch-1 loop at the active site due to weakened loop-divalent metal interactions.

In contrast to WT M761-2R, the S237C mutant ATPase was fast in the presence of MgATP (0.51 ± 0.10 s^{-1}) but was strongly inhibited by F-actin (0.02 ± 0.01 s^{-1}) (Figure 2a,b). In MnATP, the S237C mutant ATPase was also fast in the absence (0.53 ± 0.12 s^{-1}) or presence of F-actin (0.53 ± 0.09 s^{-1}). On the other hand, the mutant CaATPase activity was slow (0.07 ± 0.02 s^{-1}) and was inhibited by F-actin (0.02 ± 0.01 s^{-1}). MnATPase for WT and S237C in the presence of 10 μM F-actin is not inhibited, but there is also no additional activation observed. One possibility is that F-actin binds myosin very weakly in the presence of MnATP and thus has no real effect on motor activity. Alternatively, previously published results with WT and S237C M761 constructs showed slight activation in F-actin dependent experiments in the presence of MnATP that would not be observable under our experimental conditions (Cochran et al., 2013). In addition, the lack of robust activation is unlikely due to very weak F-actin binding as the previous study showed a sufficiently tight F-actin affinity of the WT and S237C in the presence of MnATP to cause a significant amount of binding, as shown by cosedimentation results (f_b∼0.3) and F-actin dependent ATPase assays ($K_{0.5}$ = 17 μM). This is consistent with our cosedimentation assays where we observed ∼20% of motors still bound to F-actin in the presence of MnATP (Figure 1). The shallow binding curves in our previous study strongly suggest that it is not weak actin affinity that underlies poor ATPase stimulation, but that already high basal ATPase rates in the MnATP state hides the fold-stimulation seen for WT myosin in the presence of MgATP.

(a)

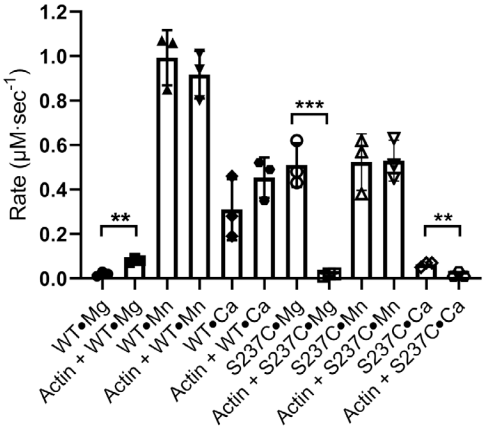

(b)

	WT (μM·s^{-1})	S237C (μM·s^{-1})
MgATP	0.02 ± 0.01	0.51 ± 0.10
MgATP + F-actin	0.08 ± 0.01	0.02 ± 0.01
MnATP	1.00 ± 0.13	0.53 ± 0.12
MnATP + F-actin	0.92 ± 0.11	0.53 ± 0.09
CaATP	0.31 ± 0.14	0.07 ± 0.02
CaATP + F-actin	0.46 ± 0.09	0.02 ± 0.01

FIGURE 2 Steady-state ATPase activity of WT and S237C myosin. The NADH-coupled assay was used to determine the ATPase activity of 0.3 μM WT or S237C myosin with 1 mM ATP and 1 mM divalent metal (Mg^{2+}, Mn^{2+}, or Ca^{2+}) in the presence or absence of 20 μM phalloidin-stabilized F-actin (n = 3). (a) Bar graph of the mean ATP turnover rates ± SD with different divalent metals. Unpaired t-tests were performed for each condition ± actin. **, $p \leq .01$; ***, $p \leq .001$. (b) Table of the mean ± SD rate of ATP turnover for each myosin and condition

The fast basal ATPase rates in the S237C mutant that we observed support our hypothesis in that the mutant has a weak divalent metal coordination of switch-1 resulting in fast opening and closing of the nucleotide pocket causing high ATPase activity. F-actin inhibition of ATP hydrolysis in MgATP is likely explained by the switch loops being stabilized in an open conformation when F-actin is bound, and thereby inhibiting switch-1 closure in the very weak metal interactions (i.e., S237C with Mg^{2+}). MnATP rescue of F-actin ATPase for the S237C mutant combined with the efficient F-actin release observed in our cosedimentation assays (Figure 1) indicate that in contrast to Mg^{2+}, the switch-1 and Mn^{2+} divalent metal interaction is strong enough to close switch-1 under strain when F-actin is bound and promote the conformational change at the F-actin binding site.

3.3 | F-actin gliding is divalent metal dependent in WT and abolished in S237C myosin

F-actin gliding assays were performed to determine the effect of the S237C mutation and metal conditions on force generation (Figure 3a). Robust F-actin motility was observed for WT M761-2R in the presence of MgATP (0.11 ± 0.01 μm/s), in good agreement with previously published work (Anson et al., 1996) (Figure 3b,c). Interestingly, in the presence of MnATP the motility for WT was inhibited approximately three-fold (0.04 ± 0.01 μm/s), and motility was abolished in the presence of CaATP (Figure 3b,c). The S237C mutant protein did not produce F-actin gliding under any condition (Figure 3b,c), and inhibited F-actin gliding when mixed with WT protein (Figure 3d).

To ensure that the inhibition of motility was not simply due to inactivation of the enzyme in the chamber, we measured the ATPase activity of WT and S237C in the gliding chambers using the NADH-coupled assay by retrieving the chamber solution and measuring the ADP concentration (Figure 3e). As a control we first observed F-actin gliding with WT M761-2R in a subset of experiments before obtaining the chamber solution to measure the ADP concentration. Given the low fraction of filament bound myosin in the gliding chamber, we expect the overall ATPase rates to resemble basal activity. Consistent with the slow ATPase rates measured in solution-based assays (Figure 2), the WT enzyme had very little ADP build up (2 ± 6 μM) in the presence of MgATP compared to MnATP (23 ± 14 μM; $p < .05$). The results for the S237C mutant were also consistent with the solution-based ATPase rates (Figure 2) in that in the presence of MgATP and MnATP large amounts of ADP were produced relative to the WT enzyme (181 ± 88 μM and 34 ± 19 μM; $p < .05$) (Figure 3e). Our results show that both WT and S237C enzymes were enzymatically active in the gliding chambers, even in reduced or absent motility. In addition, this data supports the idea that WT is highly efficient (low ATPase, fast motility) in the presence of MgATP (Figure 4a) and shows a moderate degree of uncoupling of ATP hydrolysis to force generation in the presence of MnATP.

The reduced motility of the WT construct and no motility of the S237C mutant construct in the presence of Mn^{2+} highlights the sensitivity of metal binding at the active site of myosin on force generation. It is already known that divalent metal binding significantly affects the ATPase cycle by changing the rate limiting step depending on the divalent metal at the active site (Cochran et al., 2013; Tkachev, Ge, Negrashov, & Nesmelov, 2013). Thus, even small perturbations of switch-1 loop allostery can significantly affect conformational changes throughout the motor, including the F-actin binding cleft and force generation elements. Switching metals directly destabilizes switch-1 coordination due to differences in affinity and atomic radii of the metal (Nihei & Tonomura, 1959) and may interfere with the salt bridge (R238:E459) between switch-1 and switch-2 loops, promoting faster phosphate release and increasing the rate of conformational changes in the motor (Tkachev et al., 2013). Premature loop movement and the associated effect on product release likely contribute to uncoupling of ATP turnover from force generation.

The mechanical elements linking switch loop movement and the power stroke (i.e., converter and lever arm) are unlikely interrupted in the presence of Mn^{2+} or Ca^{2+}. Muscle fibers are able to contract and produce force in the presence of excess Ca^{2+} (albeit >5-fold reduced), and rotational decay times of S1 fragments measured by transient electric birefringence aimed at detecting the degree of lever arm rotation showed differences between pre- and post-power stroke nucleotide states but no significant difference when these states were Ca^{2+} or Mg^{2+} coordinated (Polosukhina, Eden, Chinn, & Highsmith, 2000). Further evidence comes from crosslinking experiments where myosin S1 forms a converter to C-terminal crosslinked product detected as a 44 kDa fragment following trypsin digestion only in the post-power stroke state but not in the pre-power stroke state (Pliszka & Karczewska, 2002). The most direct evidence comes from fluorescence studies where the bending or straightening of the converter in the pre- and post- power stroke could be measured using intrinsic fluorescence or FRET of added fluorophores. The transition from the post-power stroke to pre-power stroke can be directly observed in the presence of Mg^{2+}, Mn^{2+}, and Ca^{2+} (Ge, Gargey, Nesmelova, & Nesmelov, 2019; Tkachev et al., 2013). Consequently, the uncoupling effect of ATPase to force generation in the presence of Mn^{2+} or Ca^{2+} cannot readily be explained by a structural uncoupling in the motor domain.

While myosin likely undergoes lever arm movement during its MnATPase and CaATPase cycles, the rate of the conformational change associated with lever arm movement and phosphate release is significantly accelerated compared to the MgATPase cycle (Cochran et al., 2013; Ikebe, Inoue, & Tonomura, 1980; Sleep, Trybus, Johnson, & Taylor, 1981; Tkachev et al., 2013). Phosphate release is accelerated to the point that the conformational change associated with ADP release becomes rate limiting or co-rate limiting. Consequently, a significant proportion of myosin may undergo the power stroke and phosphate release before reattaching to the F-actin filament. The resulting increase in futile power strokes could explain the reduced motility observed for the WT in the presence of Mn^{2+} compared to Mg^{2+} (Figure 4a,b).

Interestingly, the S237C mutant was not motile (Figure 3b,c) and surprisingly completely inhibited WT motility (Figure 3d), even in the presence of Mn^{2+}. The rate limiting steps of the S237C basal

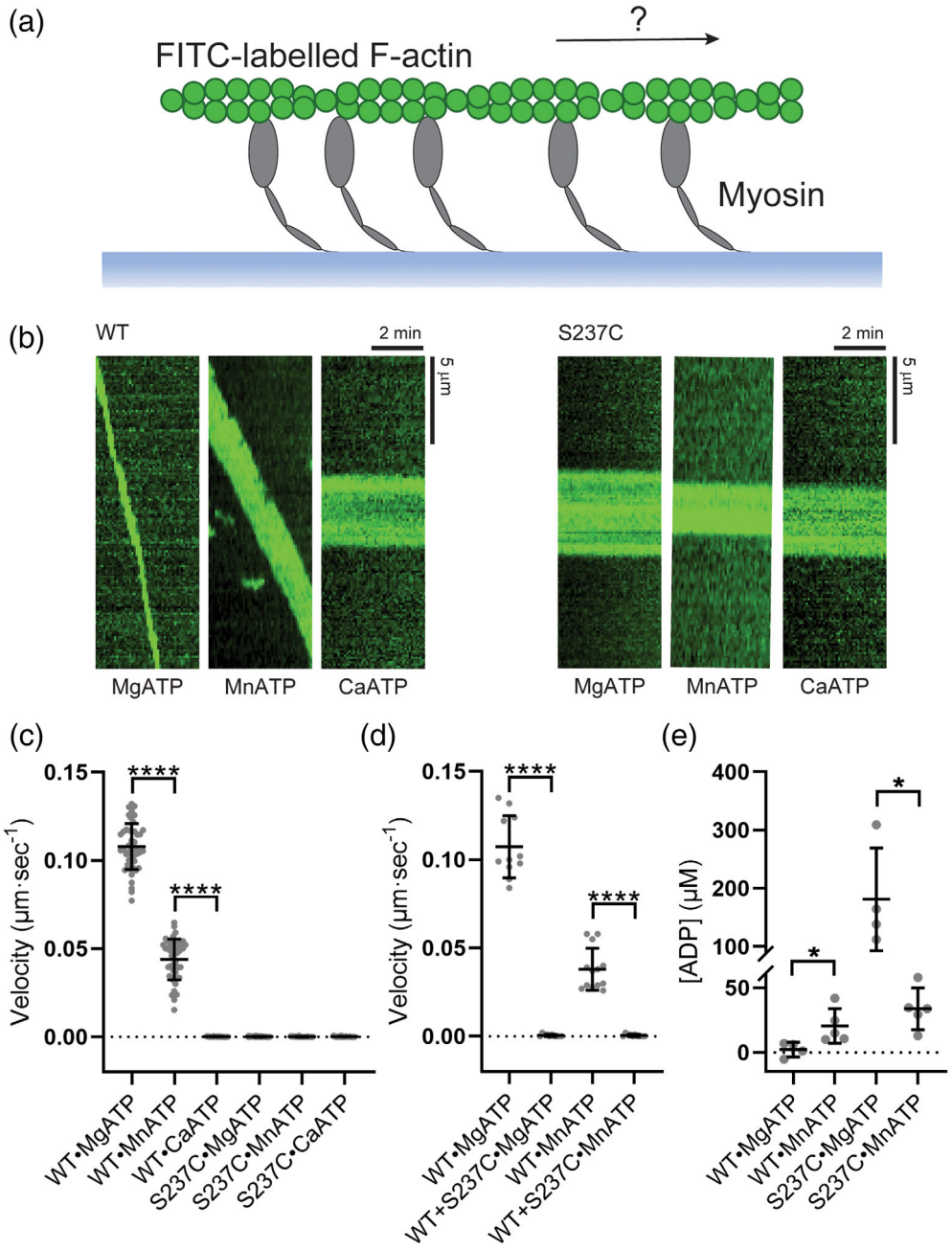

FIGURE 3 F-actin gliding by WT and S237C myosin under various metal conditions. (a) Schematic showing myosin immobilized on a microscope glass chamber and FITC-labeled F-actin bound to myosin before addition of divalent metal and ATP to induce gliding. (b) Representative kymographs of WT and S237C bound F-actin filaments in the different ATP and divalent metal compositions. (c) Scatterplot of the gliding velocity of individual actin filaments with the mean ± *SD* indicated. For each condition, gliding velocities were calculated from the slope of 10 filament kymographs per gliding chamber from five separate experiments (n = 50). WT(MgATP) = 0.11 ± 0.01 μm s^{-1}, WT(MnATP) = 0.04 ± 0.01 μm s^{-1}. For all other conditions gliding was not detected. An unpaired t-test was performed to test significance between the indicated conditions. ****$p \leq .0001$. (d) F-actin gliding velocity of individual actin filaments with the mean ± *SD* indicated of WT with and without S237C under MgATP (n = 2) and MnATP (n = 3) conditions. A minimum of 10 F-actin filaments were tracked per condition per experiment. Experiments were performed as described with WT and S237C mixtures varying from 1:1 to 5:2 ratios. WT(MgATP) = 0.11 ± 0.02 μm s^{-1}, WT(MnATP) = 0.04 ± 0.01 μm s^{-1}. For all other conditions gliding was not detected. An unpaired t-test was performed to test significance between the indicated conditions. ****$p \leq .0001$. (e) F-actin gliding chambers were filled with the NADH-coupled system and incubated at 25°C for 45 min before the solution was extracted and the amount of ADP produced measured. The amount of ADP produced in each chamber is graphed as a scatter plot with the mean ± *SD* indicated. WT(MgATP) = 2 ± 6 μM (n = 4), WT(MnATP) = 20 ± 13 μM (n = 5), S237C(MgATP) = 181 ± 88 μM (n = 4), S237C(MnATP) = 34 ± 16 μM (n = 5). An unpaired t-test was performed to test significance between the indicated conditions. *$p < .05$ [Color figure can be viewed at wileyonlinelibrary.com]

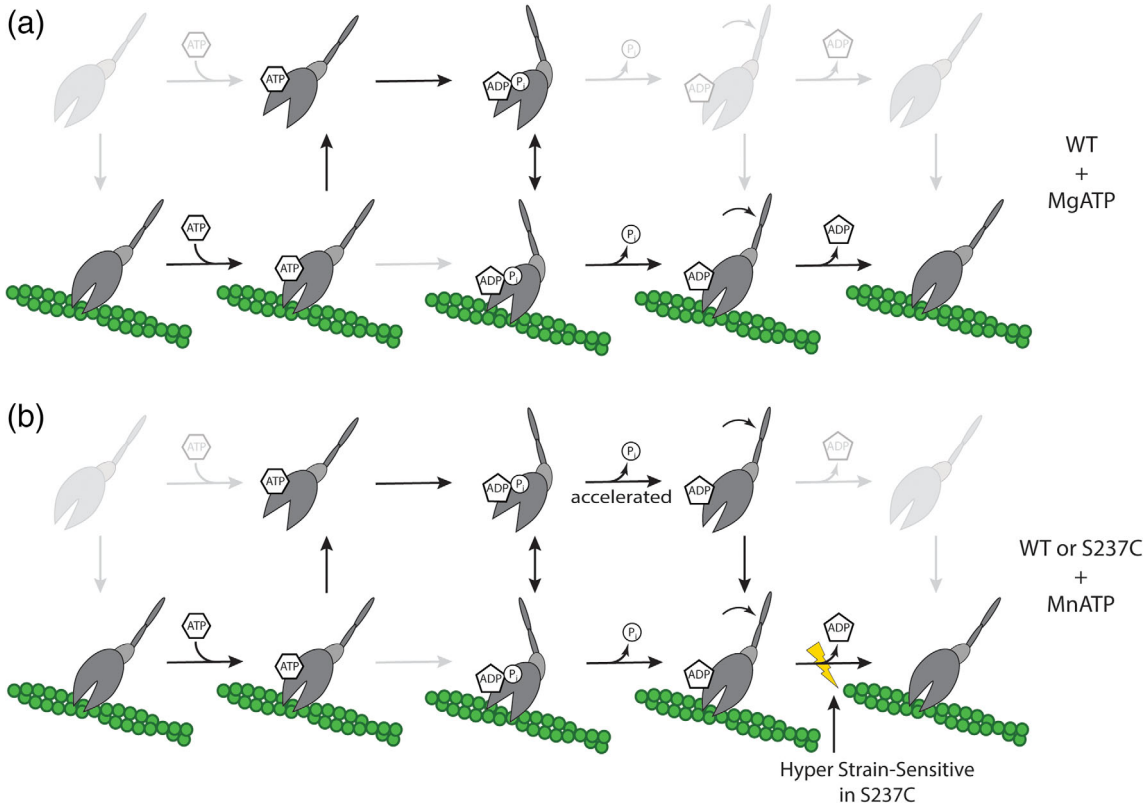

FIGURE 4 Models of ATPase cycle and force generation for myosin II. Kinetic models for myosin II motor constructs (gray) as they bind and hydrolyze ATP and release products in the presence of F-actin filaments (green). Main kinetic pathways are highlighted. The major portion of the power stroke occurs with phosphate release and is highlighted by a curved arrow. (a) Model for the WT MgATPase cycle. The conformational change that leads to tight F-actin binding intermediate, the power stroke, and P_i release limits both the basal and F-actin stimulated cycles (Gyimesi et al., 2008; Stein, Chock, & Eisenberg, 1984). Therefore, the dominant species in the ATPase cycle is the weak ADP-P_i state, and the power stroke occurs primarily when bound to F-actin (productive). (b) Model for the WT and S237C MnATPase cycles. The conformational changes that are associated with P_i and ADP release limit the basal cycle while only the conformational change associated with P_i release limits the actomyosin cycle. Consequently, a significant fraction will undergo the power stroke off the filament (futile). We suggest that ADP release is hyper strain sensitive in the S237C and leads to inhibition of force generation along the F-actin filament [Color figure can be viewed at wileyonlinelibrary.com]

MnATPase cycle were the same as WT (Cochran et al., 2013). In addition, the cosedimentation assays showed similar weak F-actin binding as the WT (Figure 1), suggesting a similar rate limiting step for the actomyosin ATPase cycle. Consequently, the lack of motility for S237C MnATPase cannot easily be explained by our solution-based assays alone. Unlike our solution-based ATPase and cosedimentation assays, myosin is under strain in the motility assays (Kron et al., 1991). This strain is unassisted by load as gliding velocities correlate well with unloaded shortening velocities in muscle. Both muscle and non-muscle myosin II have strain sensitive ADP release steps where ADP release is slowed in the presence of strain, allowing prolonged tight F-actin binding to resist detachment (Kovacs, Thirumurugan, Knight, & Sellers, 2007; Mansson, 2010; Nyitrai & Geeves, 2004; Siththanandan, Donnelly, & Ferenczi, 2006; West et al., 2009). Therefore, at the high motor density the velocity of F-actin sliding in our motility assays was determined by the ADP release limited rate of actomyosin complex dissociation (Brizendine et al., 2017; Nyitrai et al., 2006; Siemankowski, Wiseman, & White, 1985; Weiss, Rossi, Pellegrino, Bottinelli, & Geeves, 2001; Yengo, Takagi, & Sellers, 2012). In addition, Mg^{2+} directly affects ADP release kinetics for myosin II, suggesting that divalent metal coordination by the switch loops may affect the strain sensitivity of ADP release (Chizhov, Hartmann, Hundt, & Tsiavaliaris, 2013; Swenson et al., 2014). We therefore propose that interfering with divalent metal coordination, by mutating switch-1 S237C, produced a more strain sensitive motor (Figure 4b). This exaggerated strain sensitivity may allow F-actin bound motors in the gliding assay to actively inhibit motility. Our model for the S237C mutant in the presence of Mn^{2+} is similar to WT in the presence of Mn^{2+}, where a fraction of the motor undergoes futile power strokes (Figure 4b). However, the fraction of S237C undergoing the power stroke while bound to F-actin, and any other motors bound to the same filament, would experience exaggerated strain-dependent slowing of ADP release post-power stroke, which leads to an increase in motor-filament affinity and prolonged binding. This effect would be elevated when mixed with WT where strain is increased on the S237C motors when bound to the same filament. Therefore, we

propose that exaggerated strain sensitivity of S237C may allow F-actin bound motors in the gliding assay to actively inhibit motility (Figure 4b). Alternatively, S237C may inhibit motility due to post-power stroke F-actin attachment of a significant proportion of motors that then create a drag force. The WT may escape this fate in the presence of MnATP due to two-fold faster ADP release compared to S237C (Cochran et al., 2013). Faster ADP release would decrease time spent in the post-power stroke state. Future experiments will be key to testing our model and uncovering inhibition of motility by S237C.

F-actin dissociation (in solution) was significantly slowed for WT in the presence of Ca^{2+} and for S237C in the presence of Mg^{2+} and Ca^{2+} (Cochran et al., 2013; Ge et al., 2019; Tkachev et al., 2013). Under these conditions, there was unusually tight F-actin binding and F-actin inhibited ATP turnover (Figures 1 and 2, Cochran et al., 2013). We proposed previously that this inhibitory effect was due to the weakened interaction between switch-1 and divalent metal, slowing switch loop closure when the bound actin stabilizes the open conformation (Cochran et al., 2013). This explains dramatic weakening of ATP binding, which would cause a slow switch-1 induced opening of the F-actin cleft leading to the observed slowed ATP induced actomyosin dissociation. The slowing of F-actin dissociation would have an increased effect in motility assays where sliding velocity was already limited by the rate of detachment. Since detachment limits gliding velocity, it is unsurprising that higher duty ratios (time spent tightly bound to F-actin) correlate with slower motors (Bloemink & Geeves, 2011). We propose that the significantly slowed actin dissociation contributes to inhibition of motility in our assays, especially for WT in the presence of Ca^{2+}.

It is worth noting that while the weakening of nucleotide binding and decrease in ATP-dependent actin dissociation was a general feature of WT CaATPase activity; the extent varies by construct and condition. The *D. discoideum* M761 construct has weakened nucleotide affinity to the extent that F-actin binding has a slight inhibitory effect (Cochran et al., 2013), while for the M758 construct, F-actin stimulates its CaATPase less than two-fold (Korman, Anderson, Prochniewicz, Titus, & Thomas, 2006; Tkachev et al., 2013), and skeletal muscle myosin stimulation varies from as low as 1.5-fold to as high as 22-fold (Ge et al., 2019; Nihei & Tonomura, 1959; Peyser, Ajtai, Werber, Burghardt, & Muhlrad, 1997). In addition, muscle fibers are reported to produce (reduced) force in the presence of excess Ca^{2+} (Polosukhina et al., 2000). Consequently, other constructs likely vary in their duty ratios and possibly strain sensitivity in the presence of Ca^{2+} and may be capable of F-actin motility.

Together, our results strongly support the hypothesis that stable active site closure via switch-1 not only regulates ATP turnover and F-actin binding, but also regulates the coupling ATP turnover to force generation along F-actin. Hence, interfering with metal coordination by exchanging divalent metals or mutation uncouples actin-activated ATPase from force generation by increasing the rate of ATP hydrolysis while inhibiting motility.

One interesting outcome of our study with myosin illustrates differences in the coupling between ATP hydrolysis and force production with the structurally related kinesin superfamily. Our observations show that while both myosins and kinesins share a similar fold and active site components (i.e., switch-1, switch-2, P-loop), their sensitivity to switch-1 divalent metal coordination and coupling to filament binding and productive force generation are clearly different. For kinesins, Mn^{2+} structurally and functionally replaced Mg^{2+} as a cofactor for ATP hydrolysis (Cochran, Zhao, Wilcox, & Kull, 2012). In WT kinesin, microtubule gliding velocities as well as basal and microtubule stimulated ATPase rates were similar with either Mn^{2+} or Mg^{2+}, unlike in myosin where the basal ATPase activity was stimulated by MnATP but not by MgATP. In addition, the switch-1 serine to cysteine mutant in kinesin is able to rescue ATP hydrolysis rates and partially rescue gliding velocity rates in the presence of Mn^{2+}, in contrast to myosin where the cysteine mutant was unable to generate motility under any conditions. This suggests that filament binding and force generation in kinesins are less sensitive to switch-1 and divalent metal coordination than in myosins and that the coupling between these elements is less stable in myosins. Given the difference between the kinesin and myosin superfamilies, sensitivity of protein function to divalent metal coordination is likely specific among other P-loop containing NTPases. Since P-loop containing NTPases comprise the most abundant and diverse group of predicted gene products (Koonin, Wolf, & Aravind, 2000), probing the effect of divalent metal coordination on NTPase activity and biological functions using this metal-switch system is a promising approach to uncover mechanistic details of a large group of diverse proteins.

ACKNOWLEDGMENTS

We thank the Manstein Lab for their generous provision of the pDXA-3H:M761-2R plasmid. We thank Stephanie Ems-McClung and members of the Walczak Lab for valuable discussion, comments, and guidance on the manuscript. We thank the dictyBase for providing the *Dictyostelium discoideum* cell line as well as relevant references for protocols. We thank the Yu-Li Wang lab for making their actin purification protocols available to us. This work is supported by NSF Grant MCB 1614514. The Light Microscopy Imaging Center is supported in part by the Office of the Vice Provost for Research, College of Arts and Sciences, Indiana School of Medicine-Bloomington, and the School of Optometry at Indiana University.

DATA AVAILABILITY STATEMENT

Data sharing not applicable to this article as no datasets were generated or analysed during the current study

ORCID

Claire E. Walczak https://orcid.org/0000-0002-7378-2133

REFERENCES

Anson, M., Geeves, M. A., Kurzawa, S. E., & Manstein, D. J. (1996). Myosin motors with artificial lever arms. *The EMBO Journal*, *15*(22), 6069–6074. https://doi.org/10.1002/j.1460-2075.1996.tb00995.x

Bloemink, M. J., & Geeves, M. A. (2011). Shaking the myosin family tree: Biochemical kinetics defines four types of myosin motor. *Seminars in*

Cell & Developmental Biology, *22*(9), 961–967. https://doi.org/10.1016/j.semcdb.2011.09.015

Bobkov, A. A., Sutoh, K., & Reisler, E. (1997). Nucleotide and actin binding properties of the isolated motor domain from Dictyostelium discoideum myosin. *Journal of Muscle Research and Cell Motility*, *18*(5), 563–571. https://doi.org/10.1023/a:1018667319386

Brizendine, R. K., Sheehy, G. G., Alcala, D. B., Novenschi, S. I., Baker, J. E., & Cremo, C. R. (2017). A mixed-kinetic model describes unloaded velocities of smooth, skeletal, and cardiac muscle myosin filaments in vitro. *Science Advances*, *3*(12), eaao2267. https://doi.org/10.1126/sciadv.aao2267

Burke, M., Reisler, E., & Harrington, W. F. (1973). Myosin ATP hydrolysis: A mechanism involving a magnesium chelate complex. *Proceedings of the National Academy of Sciences of the United States of America*, *70* (12), 3793–3796. https://doi.org/10.1073/pnas.70.12.3793

Chizhov, I., Hartmann, F. K., Hundt, N., & Tsiavaliaris, G. (2013). Global fit analysis of myosin-5b motility reveals thermodynamics of Mg2+-sensitive acto-myosin-ADP states. *PLoS One*, *8*(5), e64797. https://doi.org/10.1371/journal.pone.0064797

Cochran, J. C. (2015). Kinesin motor enzymology: Chemistry, structure, and physics of nanoscale molecular machines. *Biophysical Reviews*, *7* (3), 269–299. https://doi.org/10.1007/s12551-014-0150-6

Cochran, J. C., Thompson, M. E., & Kull, F. J. (2013). Metal switch-controlled myosin II from Dictyostelium discoideum supports closure of nucleotide pocket during ATP binding coupled to detachment from actin filaments. *The Journal of Biological Chemistry*, *288*(39), 28312–28323. https://doi.org/10.1074/jbc.M113.466045

Cochran, J. C., Zhao, Y. C., Wilcox, D. E., & Kull, F. J. (2012). A metal switch for controlling the activity of molecular motor proteins. *Nature Structural & Molecular Biology*, *19*(1), 122–127. https://doi.org/10.1038/nsmb.2190

Conibear, P. B., Bagshaw, C. R., Fajer, P. G., Kovacs, M., & Malnasi-Csizmadia, A. (2003). Myosin cleft movement and its coupling to actomyosin dissociation. *Nature Structural Biology*, *10*(10), 831–835. https://doi.org/10.1038/nsb986

De La Cruz, E. M., Sweeney, L. H., & Ostap, M. E. (2000). ADP inhibition of myosin V ATPase activity. *Biophysical Journal*, *79*(3), 1524–1529. https://doi.org/10.1016/S0006-3495(00)76403-4

Fischer, S., Windshugel, B., Horak, D., Holmes, K. C., & Smith, J. C. (2005). Structural mechanism of the recovery stroke in the myosin molecular motor. *Proceedings of the National Academy of Sciences of the United States of America*, *102*(19), 6873–6878. https://doi.org/10.1073/pnas.0408784102

Gaudet, P., Pilcher, K. E., Fey, P., & Chisholm, R. L. (2007). Transformation of Dictyostelium discoideum with plasmid DNA. *Nature Protocols*, *2*(6), 1317–1324. https://doi.org/10.1038/nprot.2007.179

Ge, J., Gargey, A., Nesmelova, I. V., & Nesmelov, Y. E. (2019). CaATP prolongs strong actomyosin binding and promotes futile myosin stroke. *Journal of Muscle Research and Cell Motility*, *40*(3–4), 389–398. https://doi.org/10.1007/s10974-019-09556-4

Gilbert, S. P., Webb, M. R., Brune, M., & Johnson, K. A. (1995). Pathway of processive ATP hydrolysis by kinesin. *Nature*, *373*(6516), 671–676. https://doi.org/10.1038/373671a0

Gyimesi, M., Kintses, B., Bodor, A., Perczel, A., Fischer, S., Bagshaw, C. R., & Malnasi-Csizmadia, A. (2008). The mechanism of the reverse recovery step, phosphate release, and actin activation of Dictyostelium myosin II. *The Journal of Biological Chemistry*, *283*(13), 8153–8163. https://doi.org/10.1074/jbc.M708863200

Hass, L. F., Boyer, P. D., & Reynard, A. M. (1961). Studies on possible phosphoryl enzyme formation in catalysis by hexokinase, pyruvate kinase, and glucose 6-phosphatase. *The Journal of Biological Chemistry*, *236*(8), 2284–2291.

Hiratsuka, T. (1994). Nucleotide-induced closure of the ATP-binding pocket in myosin subfragment-1. *The Journal of Biological Chemistry*, *269*(44), 27251–27257.

Holmes, K. C., Angert, I., Kull, F. J., Jahn, W., & Schroder, R. R. (2003). Electron cryo-microscopy shows how strong binding of myosin to actin releases nucleotide. *Nature*, *425*(6956), 423–427. https://doi.org/10.1038/nature02005

Ikebe, M., Inoue, A., & Tonomura, Y. (1980). Reaction mechanism of Mn2+-ATPase of acto-H-meromyosin in 0.1 M KCl at 5 degrees C: Evidence for the Lymn-Taylor mechanism. *Journal of Biochemistry*, *88*(6), 1653–1662. https://doi.org/10.1093/oxfordjournals.jbchem.a133141

Imamura, K., Tada, M., & Tonomura, Y. (1966). The pre-steady state of the myosin—adenosine triphosphate system. IV. Liberation of ADP from the myosin—ATP system and effects of modifiers on the phosphorylation of myosin. *Journal of Biochemistry*, *59*(3), 280–289.

Kliche, W., Fujita-Becker, S., Kollmar, M., Manstein, D. J., & Kull, F. J. (2001). Structure of a genetically engineered molecular motor. *The EMBO Journal*, *20*(1–2), 40–46. https://doi.org/10.1093/emboj/20.1.40

Kobayashi, M., Ramirez, B. E., & Warren, C. M. (2019). Interplay of actin, ADP and Mg(2+) interactions with striated muscle myosin: Implications of their roles in ATPase. *Archives of Biochemistry and Biophysics*, *662*, 101–110. https://doi.org/10.1016/j.abb.2018.12.004

Koonin, E. V., Wolf, Y. I., & Aravind, L. (2000). Protein fold recognition using sequence profiles and its application in structural genomics. *Advances in Protein Chemistry*, *54*, 245–275. https://doi.org/10.1016/s0065-3233(00)54008-x

Koppole, S., Smith, J. C., & Fischer, S. (2007). The structural coupling between ATPase activation and recovery stroke in the myosin II motor. *Structure*, *15*(7), 825–837. https://doi.org/10.1016/j.str.2007.06.008

Korman, V. L., Anderson, S. E., Prochniewicz, E., Titus, M. A., & Thomas, D. D. (2006). Structural dynamics of the actin-myosin interface by site-directed spectroscopy. *Journal of Molecular Biology*, *356*(5), 1107–1117. https://doi.org/10.1016/j.jmb.2005.10.024

Kovacs, M., Thirumurugan, K., Knight, P. J., & Sellers, J. R. (2007). Load-dependent mechanism of nonmuscle myosin 2. *Proceedings of the National Academy of Sciences of the United States of America*, *104*(24), 9994–9999. https://doi.org/10.1073/pnas.0701181104

Kron, S. J., Toyoshima, Y. Y., Uyeda, T. Q., & Spudich, J. A. (1991). Assays for actin sliding movement over myosin-coated surfaces. *Methods in Enzymology*, *196*, 399–416. https://doi.org/10.1016/0076-6879(91)96035-p

Kull, F. J., & Endow, S. A. (2002). Kinesin: Switch I & II and the motor mechanism. *Journal of Cell Science*, *115*, 15–23.

Kull, F. J., Sablin, E. P., Lau, R., Fletterick, R. J., & Vale, R. D. (1996). Crystal structure of the kinesin motor domain reveals a structural similarity to myosin. *Nature*, *380*(6574), 550–555. https://doi.org/10.1038/380550a0

Kull, F. J., Vale, R. D., & Fletterick, R. J. (1998). The case for a common ancestor: Kinesin and myosin motor proteins and G proteins. *Journal of Muscle Research and Cell Motility*, *19*(8), 877–886. https://doi.org/10.1023/a:1005489907021

Kurzawa, S. E., & Geeves, M. A. (1996). A novel stopped-flow method for measuring the affinity of actin for myosin head fragments using microgram quantities of protein. *Journal of Muscle Research and Cell Motility*, *17*(6), 669–676. https://doi.org/10.1007/BF00154061

Kurzawa, S. E., Manstein, D. J., & Geeves, M. A. (1997). Dictyostelium discoideum myosin II: Characterization of functional myosin motor fragments. *Biochemistry*, *36*(2), 317–323. https://doi.org/10.1021/bi962166b

Llinas, P., Isabet, T., Song, L., Ropars, V., Zong, B., Benisty, H., … Houdusse, A. (2015). How actin initiates the motor activity of myosin. *Developmental Cell*, *33*(4), 401–412. https://doi.org/10.1016/j.devcel.2015.03.025

Lymn, R. W., & Taylor, E. W. (1971). Mechanism of adenosine triphosphate hydrolysis by actomyosin. *Biochemistry*, *10*(25), 4617–4624. https://doi.org/10.1021/bi00801a004

Malik, M. N., Marchioli, L., & Martonosi, A. (1972). The effect of divalent metal ions on the ATPase activity and ADP binding of H-meromyosin. *Archives of Biochemistry and Biophysics*, *153*(1), 147–154. https://doi.org/10.1016/0003-9861(72)90430-4

Mansson, A. (2010). Actomyosin-ADP states, interhead cooperativity, and the force-velocity relation of skeletal muscle. *Biophysical Journal*, *98*(7), 1237–1246. https://doi.org/10.1016/j.bpj.2009.12.4285

Muretta, J. M., Rohde, J. A., Johnsrud, D. O., Cornea, S., & Thomas, D. D. (2015). Direct real-time detection of the structural and biochemical events in the myosin power stroke. *Proceedings of the National Academy of Sciences of the United States of America*, *112*(46), 14272–14277. https://doi.org/10.1073/pnas.1514859112

Naber, N., Malnasi-Csizmadia, A., Purcell, T. J., Cooke, R., & Pate, E. (2010). Combining EPR with fluorescence spectroscopy to monitor conformational changes at the myosin nucleotide pocket. *Journal of Molecular Biology*, *396*(4), 937–948. https://doi.org/10.1016/j.jmb.2009.12.035

Nihei, T., & Tonomura, Y. (1959). Kinetic analysis of the myosin B-adenosine-triphosphatase system*. *Journal of Biochemistry*, *46*(3), 305–319. https://doi.org/10.1093/jb/46.3.305

Nyitrai, M., & Geeves, M. A. (2004). Adenosine diphosphate and strain sensitivity in myosin motors. *Philosophical Transactions of the Royal Society of London. Series B, Biological Sciences*, *359*(1452) 1867-1877, 1867–1877. https://doi.org/10.1098/rstb.2004.1560

Nyitrai, M., Rossi, R., Adamek, N., Pellegrino, M. A., Bottinelli, R., & Geeves, M. A. (2006). What limits the velocity of fast-skeletal muscle contraction in mammals? *Journal of Molecular Biology*, *355*(3), 432–442. https://doi.org/10.1016/j.jmb.2005.10.063

Peyser, Y. M., Ajtai, K., Werber, M. M., Burghardt, T. P., & Muhlrad, A. (1997). Effect of metal cations on the conformation of myosin subfragment-1-ADP-phosphate analog complexes: A near-UV circular dichroism study. *Biochemistry*, *36*(17), 5170–5178. https://doi.org/10.1021/bi970255y

Pliszka, B., & Karczewska, E. (2002). Changes at the interface of the N- and C-terminal parts of the heavy chain of myosin subfragment 1. *Biochimica et Biophysica Acta*, *1594*(2), 307–312. https://doi.org/10.1016/s0167-4838(01)00322-3

Polosukhina, K., Eden, D., Chinn, M., & Highsmith, S. (2000). CaATP as a substrate to investigate the myosin lever arm hypothesis of force generation. *Biophysical Journal*, *78*(3), 1474–1481. https://doi.org/10.1016/S0006-3495(00)76700-2

Robert-Paganin, J., Pylypenko, O., Kikuti, C., Sweeney, H. L., & Houdusse, A. (2020). Force generation by myosin motors: A structural perspective. *Chemical Reviews*, *120*(1), 5–35. https://doi.org/10.1021/acs.chemrev.9b00264

Sack, S., Kull, F. J., & Mandelkow, E. (1999). Motor proteins of the kinesin family. Structures, variations, and nucleotide binding sites. *European Journal of Biochemistry*, *262*(1), 1–11. https://doi.org/10.1046/j.1432-1327.1999.00341.x

Schindelin, J., Arganda-Carreras, I., Frise, E., Kaynig, V., Longair, M., Pietzsch, T., … Cardona, A. (2012). Fiji: An open-source platform for biological-image analysis. *Nature Methods*, *9*(7), 676–682. https://doi.org/10.1038/nmeth.2019

Siemankowski, R. F., Wiseman, M. O., & White, H. D. (1985). ADP dissociation from actomyosin subfragment 1 is sufficiently slow to limit the unloaded shortening velocity in vertebrate muscle. *Proceedings of the National Academy of Sciences of the United States of America*, *82*(3), 658–662. https://doi.org/10.1073/pnas.82.3.658

Siththanandan, V. B., Donnelly, J. L., & Ferenczi, M. A. (2006). Effect of strain on actomyosin kinetics in isometric muscle fibers. *Biophysical Journal*, *90*(10), 3653–3665. https://doi.org/10.1529/biophysj.105.072413

Sleep, J. A., Trybus, K. M., Johnson, K. A., & Taylor, E. W. (1981). Kinetic studies of normal and modified heavy meromyosin and subfragment-1. *Journal of Muscle Research and Cell Motility*, *2*, 373–399. https://doi.org/10.1007/BF00711966

Spudich, J. A., & Watt, S. (1971). The regulation of rabbit skeletal muscle contraction. I. Biochemical studies of the interaction of the tropomyosin-troponin complex with actin and the proteolytic fragments of myosin. *The Journal of Biological Chemistry*, *246*(15), 4866–4871.

Stein, L. A., Chock, P. B., & Eisenberg, E. (1984). The rate-limiting step in the actomyosin adenosinetriphosphatase cycle. *Biochemistry*, *23*(7), 1555–1563. https://doi.org/10.1021/bi00302a033

Swenson, A. M., Trivedi, D. V., Rauscher, A. A., Wang, Y., Takagi, Y., Palmer, B. M., … Yengo, C. M. (2014). Magnesium modulates actin binding and ADP release in myosin motors. *The Journal of Biological Chemistry*, *289*(34), 23977–23991. https://doi.org/10.1074/jbc.M114.562231

Tkachev, Y. V., Ge, J., Negrashov, I. V., & Nesmelov, Y. E. (2013). Metal cation controls myosin and actomyosin kinetics. *Protein Science*, *22*(12), 1766–1774. https://doi.org/10.1002/pro.2376

Vale, R. D. (1996). Switches, latches, and amplifiers: Common themes of G proteins and molecular motors. *The Journal of Cell Biology*, *135*(2), 291–302.

Vale, R. D., & Milligan, R. A. (2000). The way things move: Looking under the hood of molecular motor proteins. *Science*, *288*(5463), 88–95. https://doi.org/10.1126/science.288.5463.88

Weiss, S., Rossi, R., Pellegrino, M. A., Bottinelli, R., & Geeves, M. A. (2001). Differing ADP release rates from myosin heavy chain isoforms define the shortening velocity of skeletal muscle fibers. *The Journal of Biological Chemistry*, *276*(49), 45902–45908. https://doi.org/10.1074/jbc.M107434200

West, T. G., Hild, G., Siththanandan, V. B., Webb, M. R., Corrie, J. E., & Ferenczi, M. A. (2009). Time course and strain dependence of ADP release during contraction of permeabilized skeletal muscle fibers. *Biophysical Journal*, *96*(8), 3281–3294. https://doi.org/10.1016/j.bpj.2009.01.016

Woody, M. S., Winkelmann, D. A., Capitanio, M., Ostap, E. M., & Goldman, Y. E. (2019). Single molecule mechanics resolves the earliest events in force generation by cardiac myosin. *eLife*, *8*, e49266. https://doi.org/10.7554/eLife.49266

Yengo, C. M., Takagi, Y., & Sellers, J. R. (2012). Temperature dependent measurements reveal similarities between muscle and non-muscle myosin motility. *Journal of Muscle Research and Cell Motility*, *33*(6), 385–394. https://doi.org/10.1007/s10974-012-9316-7

SUPPORTING INFORMATION

Additional supporting information may be found online in the Supporting Information section at the end of this article.

How to cite this article: Walker BC, Walczak CE, Cochran JC. Switch-1 instability at the active site decouples ATP hydrolysis from force generation in myosin II. *Cytoskeleton*. 2021;78:3–13. https://doi.org/10.1002/cm.21650